Frontiers of Information Technology & Electronic Engineering
www.jzus.zju.edu.cn; engineering.cae.cn; www.springerlink.com
ISSN 2095-9184 (print); ISSN 2095-9230 (online)
E-mail: jzus@zju.edu.cn

A fast integral sliding mode control with extended state observer for position control of PMSM servo systems *

Jun-feng JIANG [1,2], Xiao-jun ZHOU [†‡1,2] , Wei ZHAO[3] , Wei LI[3] , Wen-dong ZHANG[4]

[1] *State Key Laboratory of Fluid Power and Mechatronic Systems, Zhejiang University, Hangzhou 310027, China*

[2] *Zhejiang Province Key Laboratory of Advanced Manufacturing Technology, Zhejiang University, Hangzhou 310027, China*

[3] *Northwest Institute of Mechanical and Electrical Engineering, Xianyang 712099, China*

[4] *Beijing Linkstech Technology Co., Ltd, Beijing 102200, China*

[†]E-mail: cmeesky@163.com

Received Jan. 6, 2010; Revision accepted Apr. 10, 2010; Crosschecked May 8, 2010

Abstract: The permanent magnet synchronous motor (PMSM) has been widely used in position control applications. Its performance is not satisfactory due to the internal uncertainties and external load disturbance. To enhance the control performance of PMSM systems, a new method which has a fast performance and good robustness is proposed in this paper. First, a modified integral terminal sliding mode control is developed. It has a faster sliding surface and a continuous reaching law. Then the extended state observer technique is applied to measure the internal and external disturbances. Therefore, the disturbances can be compensated by a feedforward manner. Compared with other sliding mode methods, the proposed method has a faster response and a better robustness against system disturbances. In addition, the position tracking error can converge to zero in finite time. Simulation and experimental results reveal that a fast, high-precision and robust performance is realised under the proposed control method.

Key words: Permanent magnet synchronous motor (PMSM); Sliding mode control; Extended state observer (ESO); Robust control; Motion control

https://doi.org/10.1631/FITEE.1000000 **CLC number:** TM351

1 Introduction

The permanent magnet synchronous motor (PMSM) is important in high-performance servo applications (e.g., machine tools, aviation and robots). It has the advantages such as high power density, compactness and low inertia (Chen *et al.*, 2015; Zeng *et al.*, 2002). The proportional-integral (PI) controller has been extensively used because of its easy implementation (Wang *et al.*, 2018). However, achieving a satisfying control performance for PMSM systems is unrealistic only by the PI controller (Wai, 2001; Yang *et al.*, 2017), because the PMSM is a nonlinear system. In addition, it is affected by external load disturbance and internal parameter variations in practical applications (Li *et al.*, 2015; Yu *et al.*, 2005).

To enhance the performance of PMSM servo systems, varieties of nonlinear control methods have been proposed, such as fuzzy logic control (Chaoui and Sicard, 2012), neural network control (El-Sousy, 2010), and predictive control (Zhi *et al.*, 2010). In El-Sousy (2010) and El-Sousy (2013), an intelligent neural network control method was designed to deal with the unmodeled parts of PMSM model. An adaptive fuzzy controller was developed to eliminate the interconnection effects of the PMSM in Barkat *et al.* (2011). In Nguyen and Jung (2018), a model predic-

‡ Corresponding author
ORCID: Xiao-jun ZHOU, http://orcid.org/0000-0003-2565-1398

tive control (MPC) was developed to guarantee the stability and robustness for surfaced-mounted PMSM drives. In addition, it was verified that the MPC method had fast speed-tracking capacity and low switching frequency. The above methods have improved the control performance of PMSM systems from different aspects. However, it should be noted that the design complexity and computational burden of these new methods are increased (Nguyen *et al.*, 2018). Moreover, how to generalize their designs into our application, the position control of PMSM, is a question.

The sliding mode control (SMC) has been applied widely for its fast response and robustness (Zhang, 2016) to uncertainties. In general, the following three steps must be considered to design a SMC system: the choice of a sliding mode surface, the design of a kind of reaching law and finally the determination of a control law. The conventional SMC usually has a linear sliding surface (SS). Consequently, it can only guarantee the asymptotic stability, i.e., the response error cannot converge to zero in finite time. The terminal sliding mode (TSM) control possessing a nonlinear SS was introduced in Man *et al.* (1994). Unlike conventional SMC, the TSM method can guarantee a finite-time convergence. However, the control input of TSM control is singular in some cases. To solve this problem, a non-singular TSM (NTSM) has been proposed in Feng *et al.* (2002). However, the reaching law of NTSM is discontinuous and therefore a chattering phenomenon is inevitable. The boundary layer method has been adopted to reduce the chattering level, but it can lead to an asymptotic stability. In Yu *et al.* (2005), a continuous NTSM (CNTSM) was developed by replacing the discontinuous reaching law of NTSM with a continuous one (Al-Ghanimi *et al.*, 2017). As a result, the chattering and singularity problems, which are the two main problems of the TSM control scheme (Feng *et al.*, 2014), are solved to some extent.

However, there are still two main issues relevant the usage of the CNTSM method:

(1) The nonlinear SS makes it much slower to converge in comparison with the linear one. This phenomenon occurs especially when the system state is far away from the equilibrium.

(2) A prior knowledge of the bound of lumped disturbance is required to obtain enough robustness. It is impossible in real applications. Therefore, the robustness is not satisfactory and the steady state fluctuation is inevitable (Yang *et al.*, 2013).

To enhance system performance in the presence of multiple disturbance, the extended state observer (ESO) technique has been developed (Han, 2009). It has been applied successfully in motion control of PMSM (Bobtsov *et al.*, 2017; Feng *et al.*, 2004; Su *et al.*, 2005), robotic systems (Su *et al.*, 2004) and machining processes (Wu *et al.*, 2007). It regards the lumped disturbance as a new system state and can estimate both disturbance and states (Saadaoui *et al.*, 2017). Therefore, a feedforward compensation can be introduced into the controller design. Jiang and Zhou (2019) proposed a robust and fast TSM (RFTSM) control method by combing the fast TSM control with the ESO method. Simulation results show that the RFTSM method has a fast, precise and robust performance in position tracking control of PMSM drives. However, experimental verifications are absent and the positioning performance of PMSM drives is not verified. In addition, the singularity problem is not avoided in RFTSM design.

In this paper, a fast continuous integral sliding mode (FCISM) control is proposed for PMSM systems. Then combining the FCISM control with the ESO technique, we propose a composite robust FCISM (RFCISM) method. The proposed RFCISM method remains the advantages of RFTSM such as finite-time stability and disturbance rejection capability. Besides, It can start on the sliding surface therefore the reaching phase is eliminated and a faster response can be guaranteed. In addition, the RFCISM solve the singularity problem in RFCISM control effectively. Simulation and experimental results are provided to validate the effectiveness of the proposed method.

The rest of the paper is organised as follows. Section 2 shows the control scheme design. The classical mathematical model of PMSM is built and the proposed control method is applied in Section 3. Simulation and experimental results are presented in Section 4. Finally, Section 5 gives the concluding remarks.

2 Controller design

A second-order nonlinear dynamic system with

external disturbance can be expressed as

$$\begin{cases}\dot{x}_1 = x_2 \\ \dot{x}_2 = g(x)u + f(x) + d\end{cases} \tag{1}$$

where $\boldsymbol{x}=[x_1, x_2]^{\mathrm{T}}$ is the system state vector, $g(x)$ and $f(x)$ represent nonlinear functions of x, d is the lumped disturbance consisting of both internal uncertainties and external load disturbance, and the scalar u is the control input signal. Let x_{ref} be the position reference and define the tracking error as $e=x_1-x_{ref}$. The control purpose is to obtain a control input u such that the system position output x_1 tracks the position reference fast and precisely.

2.1 FCISM controller design

The SS of NTSM introduced in Feng *et al.* (2002) can be described as

$$s = e + \beta \dot{e}^{m/n} = 0 \tag{2}$$

where $0<\beta<1$ is a design constant, and both m and n are positive odd integers satisfying $n<m<2n$. Then, the control input u does not have terms with negative fractional powers, which may lead to a singularity. However, the reaching law of NTSM has a switching term as follows

$$\dot{s} = -\eta \operatorname{sgn}(s) \tag{3}$$

where $\eta>0$ is a constant to be designed, and sgn represents the sign function. It is evident that this type of reaching law will lead to a chattering control input. To alleviate the chattering phenomenon, the boundary layer approach (Baik *et al.*, 2000) was incorporated into NTSM. However, choosing the width of boundary layer is not easy and the performance of disturbance rejection is sacrificed (Wang *et al.*, 2017).

Retaining the non-singular and finite-time SS, CNTSM control is proposed by replacing the discontinuous reaching law with a continuous one as follows

$$\dot{s} = -k_1 s - k_2 |s|^{q_0/p_0} \operatorname{sgn}(s) \tag{4}$$

where k_1 and k_2 are positive design constants, and both p_0 and q_0 are positive odd integers satisfying $p_0>q_0$. As a result, the derived control input is without any negative fractional power therefore non-singular and continuous therefore chattering-free. However, the following equation can be deduced according to (2)

$$\dot{e} = -\frac{1}{\beta^{n/m}} e^{n/m} \tag{5}$$

It is obvious that the absolute value of $\dot{e}$ is much smaller compared with $\dot{e} = -\frac{1}{\beta^{m/n}} e^{m/n}$ when e is far away from zero. In other words, the convergence rate of nonlinear SS is slower than that of linear SS. Note that the result completely reverses when e is close to zero.

A fast integral SS is designed as follows

$$s = \dot{e} + \beta_{\mathrm{I}} e^{\gamma_1} + \alpha_{\mathrm{I}} \int_0^t e^{\gamma_2}(\tau) d\tau \tag{6}$$

To obtain a fast convergence rate as mentioned above, γ_2 is defined as

$$\gamma_2 = \begin{cases} m_{\mathrm{I}} / n_{\mathrm{I}} & |e| \geq \delta \\ n_{\mathrm{I}} / m_{\mathrm{I}} & |e| \leq \delta \end{cases} \tag{7}$$

where β_{I}, α_{I}, γ_1 and γ_2 are positive parameters with $\gamma_1>1$, m_{I}, n_{I} are positive odd integers with $m_{\mathrm{I}} > n_{\mathrm{I}}$, and δ is the switching value. Combining SS (6) and reaching law (4), a novel FCISM method for system (1) is proposed as follows

$$\begin{aligned} u_0 = -g(x)^{-1} \Big[& f(x) + \beta_{\mathrm{I}} \gamma_1 e^{\gamma_1 - 1} \dot{e} + \alpha_{\mathrm{I}} e^{\gamma_2} \\ & - \ddot{x}_{ref} + k_{1\mathrm{I}} s + k_{2\mathrm{I}} |s|^{q_{0\mathrm{I}}/p_{0\mathrm{I}}} \operatorname{sgn}(s) \Big] \end{aligned} \tag{8}$$

where $k_{1\mathrm{I}}$, $k_{2\mathrm{I}}$, $q_{0\mathrm{I}}$, $p_{0\mathrm{I}}$ are the reaching law parameters of FCISM controller with $p_{0\mathrm{I}}>q_{0\mathrm{I}}$, the odd integer $q_{0\mathrm{I}}$ is modified as follows for finite-time stabilization

$$\begin{cases} q_{0\mathrm{I}} > 0 & |s| \geq 1 \\ q_{0\mathrm{I}} = 0 & |s| < 1 \end{cases} \tag{9}$$

Remark 1: The SS of conventional integral terminal sliding mode (ITSM) control in Chiu (2012) can be expressed as

$$s_{\mathrm{c}} = \dot{e} + \beta_{\mathrm{c}} e + \alpha_{\mathrm{c}} \int_0^t e^{n_{\mathrm{c}}/m_{\mathrm{c}}}(\tau) d\tau \tag{10}$$

with β_{c}, α_{c}, n_{c}, m_{c} are the same as β_{I}, α_{I}, n_{I}, m_{I} in equation (6), respectively. When the system states reach the SS (i.e., $s=s_{\mathrm{c}}=0$), the following equation can be derived from the proposed SS (6)

$$\dot{e} = -\beta_{\mathrm{I}} e^{\gamma_1} - \alpha_{\mathrm{I}} \int_0^t e^{m_{\mathrm{I}}/n_{\mathrm{I}}}(\tau) d\tau \tag{11}$$

and the following equation can be derived from equation (10)

$$\dot{e} = -\beta_{\mathrm{c}} e - \alpha_{\mathrm{c}} \int_0^t e^{n_{\mathrm{c}}/m_{\mathrm{c}}}(\tau) d\tau \tag{12}$$

Assume that $\beta_{\mathrm{I}}=\beta_{\mathrm{c}}$ and $\alpha_{\mathrm{I}}=\alpha_{\mathrm{c}}$, one can see that the absolute value of $\dot{e}$ in equation (12) is smaller compared with that of equation (11) when e is far away from zero. In other words, the convergence rate of conventional method is slower than that of the pro-

posed method when e is far away from zero. This will also be validated by the following simulations and experiments.

Remark 2: Non-singularity and fast response are two main advantages of ITSM control. We can enable the system states to start on the SS s=0 by adjusting the initial value of $\int_0^t e^{\gamma_2}(\tau)d\tau$. Therefore, reaching phase can be eliminated and fast response can be obtained. In addition, one can see from expression (8) that there is no negative fractional power in the control law. In other words, the proposed control scheme is non-singular.

2.2 RFCISM controller design

To improve the disturbance rejection property of this system, an ESO technique is incorporated to estimate the lumped disturbance. The estimated disturbance acts as a feedforward compensation term.

According to Miklosovic and Gao (2004), a second-order linear ESO for system (1) can be designed as follows

$$\begin{cases}\dot{\hat{x}}_2=\hat{d}-2p(\hat{x}_2-x_2)+g(x)u\\ \dot{\hat{d}}=-p^2(\hat{x}_2-x_2)\end{cases} \tag{13}$$

where $\hat{x}_2$ and $\hat{d}$ are the estimate of x_2 and d, respectively, and $-p$ is the desired double pole of the ESO with $-p$<0. The estimated disturbance will converge to the real lumped d asymptotically. The estimation error is defined as

$$\tilde{d}=\hat{d}-d \tag{14}$$

Note that $\hat{d}$ often contains some bounded noise in real applications and thus the estimation error is bounded by a constant

$$\left|\tilde{d}\right|<\varepsilon \tag{15}$$

with ε is a positive value.

Combing the FCISM and the ESO technique, the RFCISM method is developed as follows

$$u=u_0-g(x)^{-1}\hat{d} \tag{16}$$

Compared with the control law (8), control law (16) has a disturbance compensation term. Therefore, it has a better disturbance rejection property and a smaller steady state fluctuation.

Theorem: For system (1), if the control input u is designed as (16) and the gain satisfies $k_{2\mathrm{I}}\geq\varepsilon$, the tracking error e and its first-order derivative $\dot{e}$ will converge to zero in finite time.

Proof: Choosing a Lyapunov function as

$$V=\frac{1}{2}s^2 \tag{17}$$

Then the derivative of the Lyapunov function is

$$\begin{aligned}\dot{V}&=s\dot{s}=s(\ddot{e}+\beta_1\gamma_1e^{\gamma_1-1}\dot{e}+\alpha_1e^{\gamma_2})\\&=s\big[g(x)u+f(x)+d-\ddot{x}_{ref}\\&\quad+\beta_1\gamma_1e^{\gamma_1-1}\dot{e}+\alpha_1e^{\gamma_2}\big]\end{aligned} \tag{18}$$

Substituting control law equation (16) into equation (18) yields

$$\begin{aligned}\dot{V}&=s\Big\{g(x)\big[-g(x)^{-1}(f(x)+\beta_1\gamma_1e^{\gamma_1-1}\dot{e}+\alpha_1e^{\gamma_2}\\&\quad-\ddot{x}_{ref}+k_{1\mathrm{I}}s+k_{2\mathrm{I}}|s|^{q_{0\mathrm{I}}/p_{0\mathrm{I}}}\operatorname{sgn}(s)+\hat{d})\big]\\&\quad+f(x)+d-\ddot{x}_{ref}+\beta_1\gamma_1e^{\gamma_1-1}\dot{e}+\alpha_1e^{\gamma_2}\Big\}\\&=s\left(-k_{1\mathrm{I}}s-k_{2\mathrm{I}}|s|^{q_{0\mathrm{I}}/p_{0\mathrm{I}}}\operatorname{sgn}(s)-\tilde{d}\right)\end{aligned} \tag{19}$$

If $|s|\geq1$, equation (19) can be rewritten as

$$\begin{aligned}\dot{V}&=-k_{1\mathrm{I}}s^2-k_{2\mathrm{I}}|s|^{q_{0\mathrm{I}}/p_{0\mathrm{I}}}s\operatorname{sgn}(s)-\tilde{d}s\\&=-k_{1\mathrm{I}}s^2-k_{2\mathrm{I}}|s|^{q_{0\mathrm{I}}/p_{0\mathrm{I}}}|s|-\tilde{d}s\\&\leq-k_{1\mathrm{I}}s^2-k_{2\mathrm{I}}|s|^{q_{0\mathrm{I}}/p_{0\mathrm{I}}+1}+\left|\tilde{d}\right||s|\\&=-k_{1\mathrm{I}}s^2-\left(k_{2\mathrm{I}}|s|^{q_{0\mathrm{I}}/p_{0\mathrm{I}}}-\left|\tilde{d}\right|\right)|s|\\&\leq-k_{1\mathrm{I}}s^2-(k_{2\mathrm{I}}-\varepsilon)|s|\leq0\end{aligned} \tag{20}$$

If $|s|<1$, equation can be rewritten as

$$\begin{aligned}\dot{V}&=-k_{1\mathrm{I}}s^2-k_{2\mathrm{I}}|s|^{q_{0\mathrm{I}}/p_{0\mathrm{I}}}s\operatorname{sgn}(s)-\tilde{d}s\\&=-k_{1\mathrm{I}}s^2-k_{2\mathrm{I}}|s|-\tilde{d}s\\&\leq-k_{1\mathrm{I}}s^2-k_{2\mathrm{I}}|s|+\left|\tilde{d}\right||s|\\&=-k_{1\mathrm{I}}s^2-\left(k_{2\mathrm{I}}-\left|\tilde{d}\right|\right)|s|\leq0\end{aligned} \tag{21}$$

Therefore, the condition for Lyapunov stability is satisfied. This completes the proof.

3 Application in PMSM servo systems

Taking the rotor coordinates d-q as reference coordinates, the mathematical model of surface-mounted PMSM can be expressed as follows (Li and Liu, 2009)

$$\begin{cases} u_d = L_s\dot{i}_d - \omega_r L_s i_q + R_s i_d \\ u_q = L_s\dot{i}_q + \omega_r L_s i_d + R_s i_q + \psi_r \omega_r \\ T_e = K_t i_q \\ \dfrac{J}{n_p}\dot{\omega}_r = T_e - \dfrac{B}{n_p}\omega_r - T_L \end{cases} \tag{22}$$

where

u_d,u_q d and q axis stator voltages, respectively;
i_d, i_q d and q axis stator currents, respectively;
L_s stator inductance;
R_s stator resistance;
ψ_r the normal value of flux linkage of rotors;
ω_r electrical angular velocity of rotors;
T_e electrical magnetic torque;
n_p number of pole pairs;
K_t torque constant;
J system moment of inertia;
B viscous friction coefficient;
T_L load torque.

The three-loop control structure of PMSM systems based on field oriented vector control strategy is shown in Fig. 1. This cascade structure includes a position loop, a speed loop and two current loops. In this paper, the position loop and the speed loop are to be unified (herein after called position-speed loop). Usually, to attenuate the couplings between speed and current, d-axis reference current i_d^* is set to 0. So taking the angular position and velocity as the system state variables, the state-space model can be expressed as:

$$\begin{cases} \dot{\theta}_r = \omega_r \\ \dot{\omega}_r = \dfrac{n_p K_t}{J} i_q - \dfrac{B}{J}\omega_r - \dfrac{n_p}{J} T_L \end{cases} \tag{23}$$

where θ_r and ω_r represent the electrical angular position and velocity of rotor, respectively. Adopting the control input i_q^*, the motor state-space model can be rewritten as

$$\begin{cases} \dot{\theta}_r = \omega_r \\ \dot{\omega}_r = a i_q^* + b\omega_r + d \end{cases} \tag{24}$$

which is similar as (1) in form, where $a = \dfrac{n_p K_t}{J}$, $b = -\dfrac{B}{J}$, $d = -\dfrac{n_p K_t}{J}(i_q^* - i_q) - \dfrac{n_p}{J} T_L$ is the system disturbance.

To have a comparison, the CNTSM control is employed for PMSM systems and its control law can be described as

$$i_q^* = -a^{-1}(b\omega_r + k_1 s + k_2 s^{q_0/p_0} - \ddot{\theta}_{ref} + \beta^{-1}\frac{n}{m}\dot{e}^{2-m/n}) \tag{25}$$

where θ_{ref} is the reference position, $e = \theta_r - \theta_{ref}$, $\dot{e} = \omega_r - \dot{\theta}_{ref}$ and s is designed as (2).

According to equation (8), the FCISM control law for PMSM can be expressed as

$$\begin{aligned} i_q^* = -a^{-1}\Big[& b\omega_r + \beta_1\gamma_1 e^{\gamma_1 - 1}\dot{e} + \alpha_1 e^{\gamma_2} \\ & - \ddot{\theta}_{ref} + k_{1I} s + k_{2I}\left|s\right|^{q_{01}/p_{01}} \operatorname{sgn}(s)\Big] \end{aligned} \tag{26}$$

where s is designed as (6). According to equation (16), the RFCISM control law can be expressed as

$$\begin{aligned} i_q^* = -a^{-1}\Big[& b\omega_r + \beta_1\gamma_1 e^{\gamma_1 - 1}\dot{e} + \alpha_1 e^{\gamma_2} - \ddot{\theta}_{ref} \\ & + k_{1I} s + k_{2I}\left|s\right|^{q_{01}/p_{01}} \operatorname{sgn}(s) + \hat{d}\Big] \end{aligned} \tag{27}$$

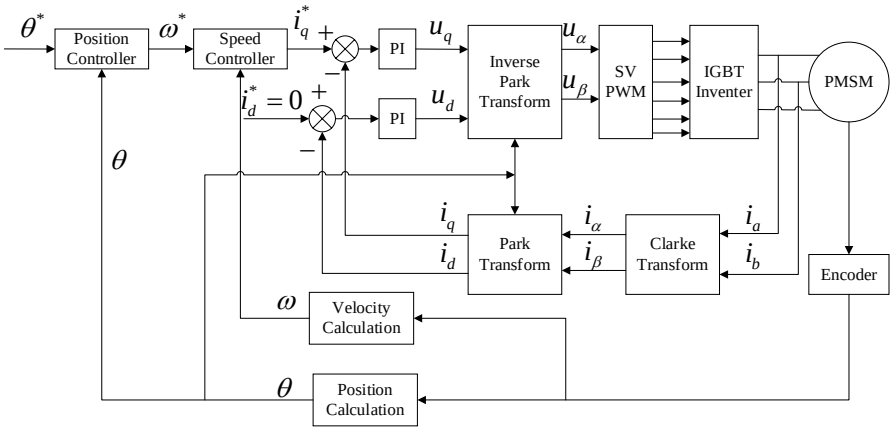

Fig. 1 Block diagram of field oriented vector control for PMSM

4 Results and discussion

To verify the performance of the proposed method, simulations and experiments are carried out in MATLAB/Simulink and DSP-based test environment, respectively. For comparisons, three methods are applied for the PMSM position control system. They are CNTSM, FCISM and RFCISM. The saturation limit of control input i_q^* is ±30 A. Note that every control algorithm obtains relative good performance by adjusting its parameters. Parameters of the PMSM are shown in Table 1.

Table 1 Parameters of the PMSM

Parameters	Values
Rated power	1.5 KW
Rated torque	14.32 Nm
Rated speed	1000 rpm
Stator resistance	1.79 Ω
Pole pairs	4
Torque constant	2.45 Nm/A
System inertia	1.792×10^{-3} kg.m^2
Viscous coefficient	9.403×10^{-5} Nm.s/rad
Stator inductance	6.68×10^{-3} H
Flux linkage	0.4083 Wb

4.1 Simulation results

The PMSM tracking system under the aforementioned three control schemes is simulated by MATLAB/Simulink R2017a. The position reference is $\theta^*=30\cos(\pi/2t)$ deg, which can lead to a relative good performance for CNTSM control. To demonstrate the disturbance rejection ability of the proposed method, external load torque T_L=30 Nm is added at t=2 s and removed at t=3 s. The PI parameters of both current loops are the same: the proportional gain Kp =150 and the integral gain Ki =750.

The parameters of CNTSM are selected as: k_1=200, k_2=200, q_0=1, p_0=5, m=9, n=5, β=1/500. The simulation results of CNTSM are shown in Fig. 2. One can see that the tracking error converges to zero in finite time and there is no singularity in the control input i_q^*. However, we find that the convergence rate is slow. In addition, there are obvious fluctuations in Fig. 2a when the external disturbance is added or removed.

The parameters of FCISM in the linear phase are: β_I=1/18, α_I=50, γ_1=1.7, k_{1I}=300, k_{2I}=300, n_I=1, m_I=5, q_{0I}=1, p_{0I}=5, δ=0.03. The simulation results of FCISM are shown in Fig. 3. It is obvious that the convergence time of FCISM is much shorter than that of CNTSM. But the fluctuations of tracking error still exist due to external disturbance. Moreover, we can see from Fig. 3b that the control input i_q^* does not act effectively to suppress the disturbance.

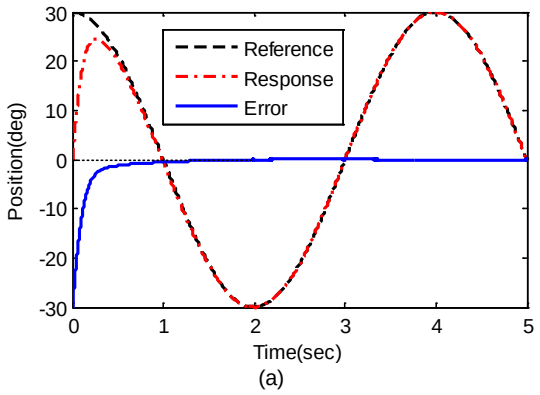

(a)

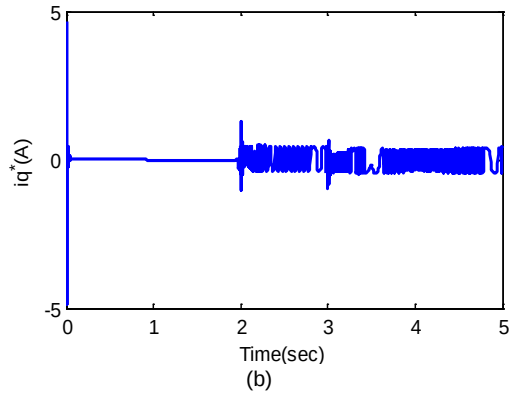

Fig. 2 Tracking performance of CNTSM (simulation). (a) Position response, (b) control input i_q^*

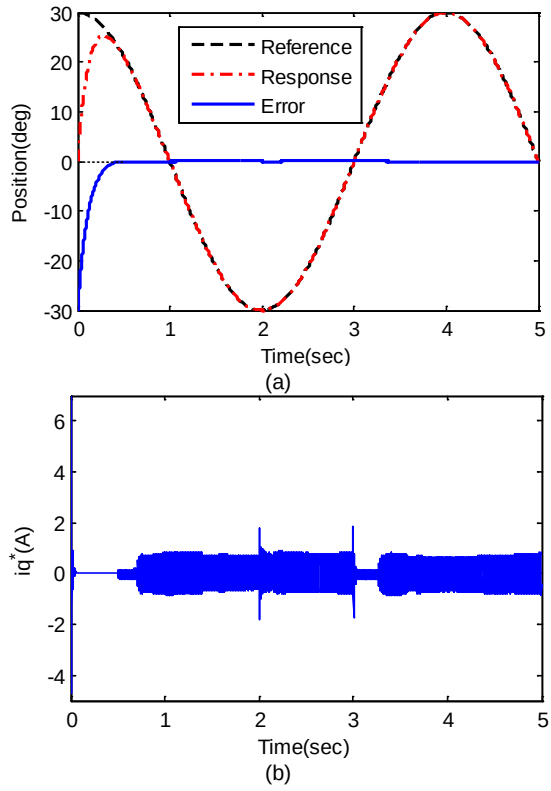

Fig. 3 Tracking performance of FCISM (simulation). (a) Position response, (b) control input i_q^*

For RFCISM, the pole of ESO is $-p=-50000$ and the other parameters are the same as those of FCISM. The simulation results of RFCISM are shown in Fig. 4. One can see that a fast and high-precision control performance is achieved. Additionally, the disturbance effect is eliminated effectively. The reason can be found in Fig. 4b and 5. We can see from Fig. 5 that the ESO can estimate disturbance accurately. Hence, the absolute value of control input can increase remarkably to depress the disturbance as shown in Fig. 4b. Fig. 6 shows the position response under RFCISM with perturbation in system inertia. $J_0=1.792\times10^{-3}$ kg.m^2 is the initial value of system inertia. It can be seen that the transient response remains fast and accurate regardless of the internal parameter variations. In addition, the tracking error of PMSM systems under flux linkage variations is shown in Fig. 7. $\psi_{r0}=0.41$Wb is the nominal value of rotor flux. It can be observed that there is almost no effect on the tracking performance under different rotor flux. Thus, we can easily conclude that the proposed method has a strong robustness against external disturbance and internal uncertainties.

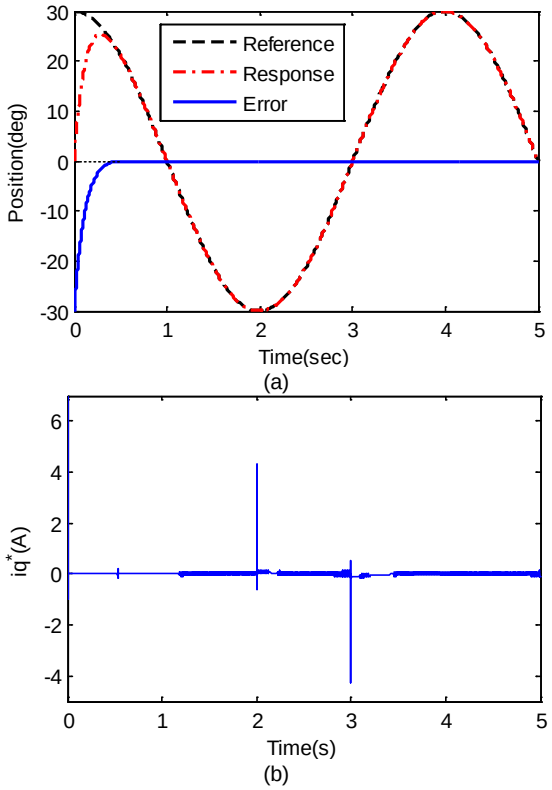

Fig. 4 Tracking performance of RFCISM (simulation). (a) Position response, (b) control input i

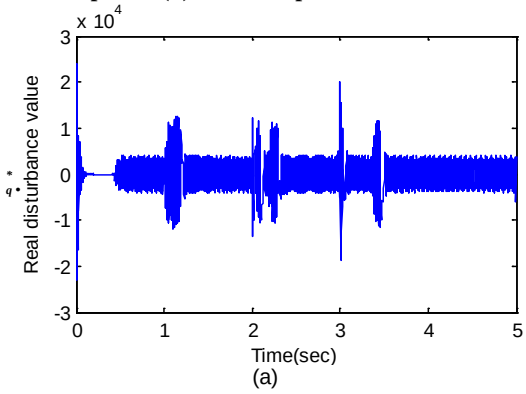

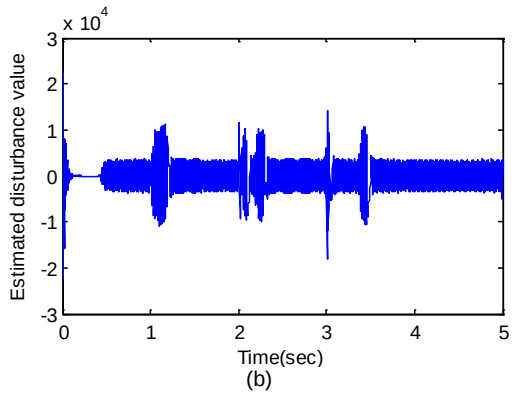

Fig. 5 Estimated disturbance values of ESO and real disturbance values(simulation). (a)Real disturbance value, (b)estimated disturbance value

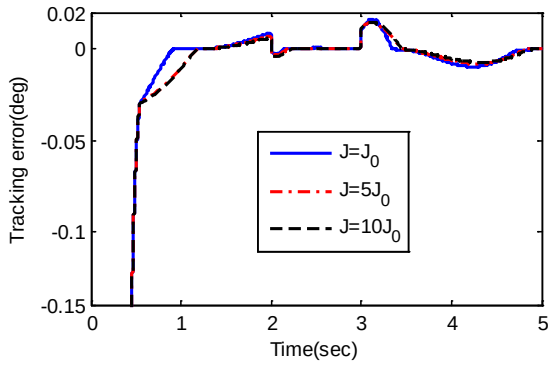

Fig. 6 Tracking performance of RFCISM under system inertia variations (simulation)

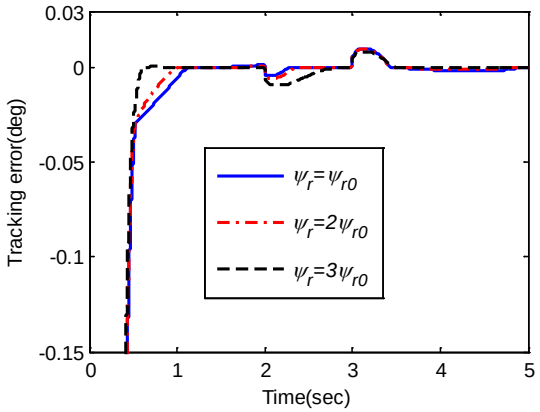

Fig. 7 Tracking performance of RFCISM under flux linkage variations (simulation)

4.2 Experimental results

To further evaluate the effectiveness of the RFCISM method, an experimental setup for position control of the PMSM was built. Fig. 8 shows the experimental test setup. The real-time emulator contains a DSP TMS320F28335PGFA. The function of it is to provide a MATLAB/Simulink programming environment. The whole algorithm, including position-speed controller, Clarke transform, inverse Park transform and so on, is implemented by MATLAB/Simulink. Then, all of those algorithms are converted into DSP code. Next, the gate drive is sent from DSP to the driver of PMSM. The experimental data can be collected on the host computer. All of the processes are supported by a real-time simulation software named Links-RT. The sample time of position-speed loop and current loop are 1 ms and 0.1 ms, respectively. An incremental position encoder is used to measure the rotor speed and absolute rotor position. Hall-effect devices are used to measure the phase currents.

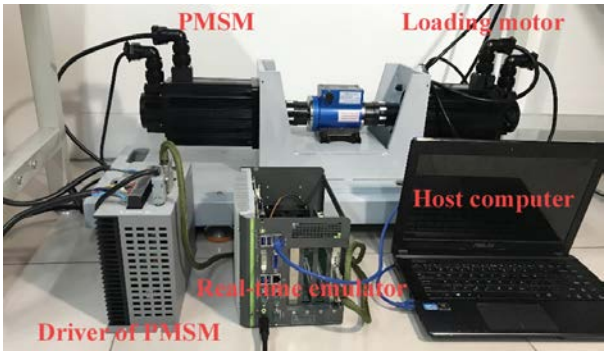

Fig. 8 Experimental test setup

The parameters of CNTSM are selected to be: k_1=150, k_2=150, q_0=1, p_0=5, m=9, n=5, β_2=1/120. The PI parameters of both current loops are the same: the proportional gain K_p =5.7 and the integral gain K_i=8.6. The parameters of FCISM are: β_1=1/180, α_1=200, γ_1=1.7, n_1=1, m_1=5,k_{11}=250, k_{21}=250, q_{01}=1, p_{01}=5, δ=1 in the nonlinear phase. The PI parameters of both current loops are the same: K_p =7.5 and K_i =12.5. For RFCISM, the pole of ESO is selected as $-p$=−35000 and the other parameters are the same as those of FCISM.

First, we demonstrate the positioning performance of the proposed RFCISM. The position reference is set to θ^*=70 deg, which can lead to a relative good performance for CNTSM control. The performances of three schemes are show in Fig. 9 and summarized in Table 2. It is obvious that all the three control schemes can achieve finite-time stabilization, but the RFCISM can depress the overshoot and shorten the settling time effectively.

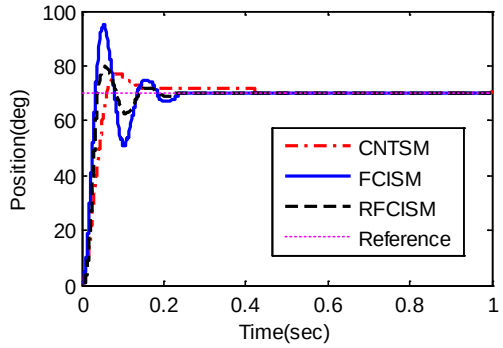

Fig. 9 Positioning performances of three methods for target position 70 deg (experiment)

Table 2 Positioning performance comparisons of three control schemes (experiment)

Control schemes	Overshoot(%)	Settling time(s)
CNTSM	10.0	0.42
FCISM	35.7	0.23
RFCISM	14.2	0.22

Then, the tracking performance of the proposed RFCISM is demonstrated. The position reference is $\theta^*=30\cos(\pi/2t)$ deg, which is the same as that of simulation. And load torque T_L=15 Nm is added at t=2 s and removed at t=2.5 s. The experimental results of CNTSM, FCISM, RFCISM are shown in Fig. 10–12, respectively. One can see that they match the simulation results well. The proposed RFCISM has a fast and precise tracking performance and a good property of robustness.

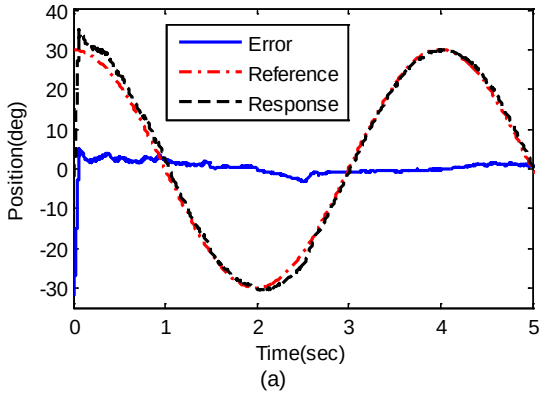

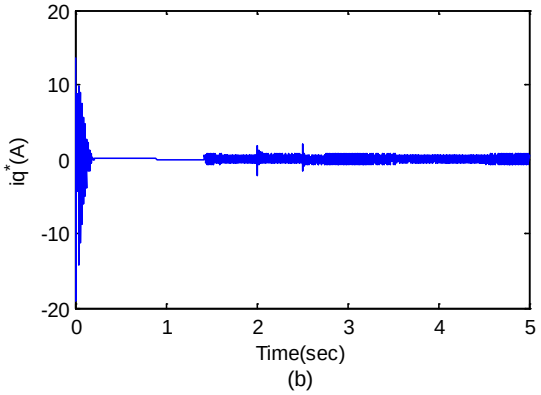

Fig. 10 Tracking performance of CNTSM (experiment). (a) Position response, (b) control input i_q^*

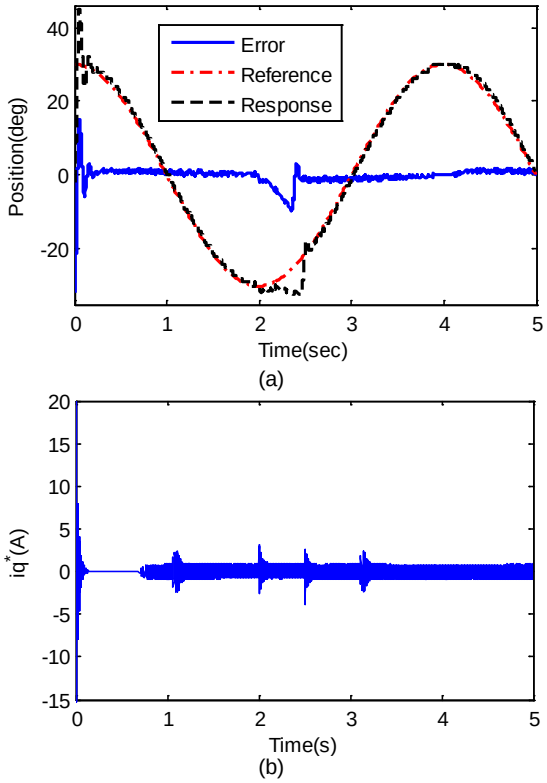

Fig. 11 Tracking performance of FCISM (experiment). (a) Position response, (b) control input i_q^*

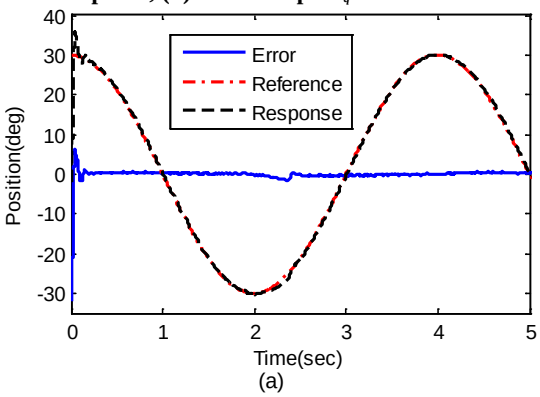

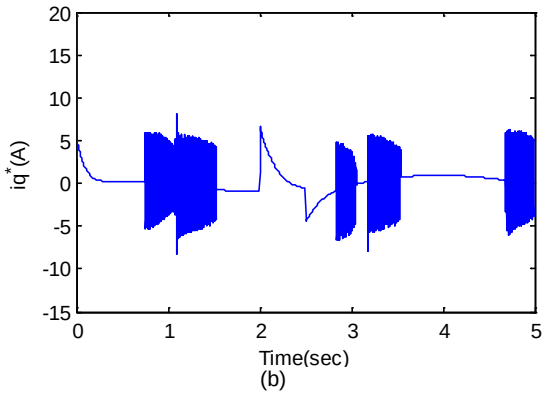

Fig. 12 Tracking performance of RFCISM (experiment). (a) Position response, (b) control input i_q^*

Next, Fig. 13 shows the tracking error of the proposed method when system inertia varies. We can see that the convergence rate becomes a little slower with the increase of the system inertia. However, the transient response remains fast and accurate regardless of the internal parameter variations. Thus, we can conclude that the proposed method has a strong robustness against internal uncertainties.

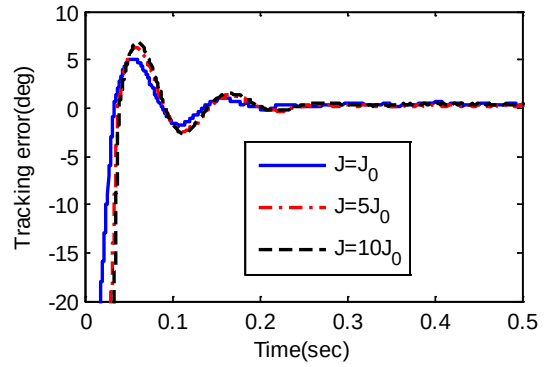

Fig. 13 Tracking performance of RFCISM with perturbations in system inertia (experiment)

Finally, to validate the tracking range of the proposed method, three different position references are adopted. They are θ^*=30cos(π/2t) deg, θ^*=60cos(π/2t) deg and θ^*=90cos(2π/3t) deg. Fig. 14 shows the experimental results. We can see that the overshoot and the settling time increase with the increase of amplification or frequency. However, the tracking performance remains desirable in all the cases. It is evident that the proposed control system has superior performance in tracking a wide range of target position.

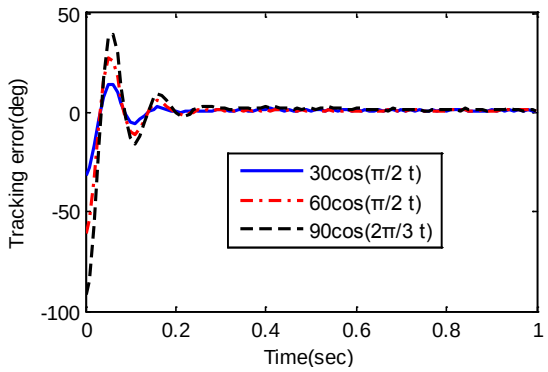

Fig. 14 Tracking errors of RFCISM for different position references (experiment)

4.3 Discussion

To make comparisons clearly, the simulation tracking performances of three methods are summarized in Table 3. It can be observed that the settling time of RFCISM is reduced by 72.9% compared with the CNTSM method. And the steady tracking error is reduced by 90.9%. The experimental tracking performances are summarized in Table 4. We can see that experimental results match simulation results well. And the settling time, steady tracking error and maximum fluctuation are reduced by 85%, 58.7% and 53.9%, respectively. Thus, we can conclude that the RFCISM control can realize faster and higher tracking performance than the conventional CNTSM method. In addition, the proposed method has superior robustness with respect to internal uncertainties and external disturbance.

Table 3 Tracking performance comparisons of three control schemes (simulation)

Control schemes	Settling time (s)	Steady tracking error (deg)
CNTSM	1.7	0.11
FCISM	0.47	0.11
RFCISM	0.46	0.01

Table 4 Tracking performance comparisons of three control schemes (experiment)

Control schemes	Settling time(s)	Steady tracking error (deg)	Maximum disturbance fluctuation (deg)
CNTSM	1.2	1.5	3.21
FCISM	0.18	1.67	3.09
RFCISM	0.18	0.62	1.48

It should be noted that there is still some chat-

tering in the control signals as shown in results. However, it is well known that power converters have only the on–off operation mode. Therefore, chattering does not cause difficulties for practical electric drives. To eliminate the chattering phenomenon in PMSM systems, the reaching law should be improved further in the next work.

5 Conclusion

A fast and robust sliding mode control is proposed for motion control of PMSM servo systems. The contributions of the proposed controller can be listed as follows

(1) The conventional integral SS is modified so that a faster convergence can be obtained.

(2) A continuous reaching law is applied in the controller design. Consequently, the chattering problem of the conventional SMC can be solved to some extent.

(3) The ESO technique is adopted to estimate and compensate system disturbances. So the disturbance rejection capability of PMSM systems can be improved remarkably.

Simulation and experimental results show that the proposed RFCISM has fast and accurate performance in both positioning and tracking. In addition, a good robustness against inertial parameter variations and external load disturbance is obtained. The new control scheme can be applied to other relevant servo systems.

References

Al-Ghanimi, A., Zheng, J., Man, Z., 2017. A fast non-singular terminal sliding mode control based on perturbation estimation for piezoelectric actuators systems. *Int. J. Contr.*, 90(3):480-491. https://dx.doi.org/10.1080/00207179.2016.1185157

Baik, I.C., Kim, K.H., Youn, M.J., 2000. Robust nonlinear speed control of PM synchronous motor using boundary layer integral sliding mode control technique. *IEEE Trans. Contr. Syst. T.*, 8(1):47-54. https://dx.doi.org/10.1109/87.817691

Barkat, S., Tlemcani, A., Nouri, H., 2011. Noninteracting Adaptive Control of PMSM Using Interval Type-2 Fuzzy Logic Systems. *IEEE Trans. Fuzzy Syst.*, 19(5): 925-936. https://dx.doi.org/10.1109/Tfuzz.2011.2152815

Bobtsov, A., Bazylev, D., Pyrkin, A., et al., 2017. A robust nonlinear position observer for synchronous motors with relaxed excitation conditions. *Int. J. Contr.*, 90(4): 813-824. https://dx.doi.org/10.1080/00207179.2016.1230229

Chaoui, H., Sicard, P., 2012. Adaptive Fuzzy Logic Control of Permanent Magnet Synchronous Machines With Nonlinear Friction. *IEEE Trans. Ind. Electron.*, 59(2): 1123-1133. https://dx.doi.org/10.1109/Tie.2011.2148678

Chen, Q.H., Wang, Q.F., Wang, T., 2015. Optimization design of an interior permanent-magnet synchronous machine for a hybrid hydraulic excavator. *Front. Inform. Technol. Electron. Eng.*, 16(11):957-968. https://dx.doi.org/10.1631/fitee.1500056

Chiu, C.S., 2012. Derivative and integral terminal sliding mode control for a class of MIMO nonlinear systems. *Automatica*, 48(2):316-326. https://dx.doi.org/10.1016/j.automatica.2011.08.055

El-Sousy, F.F.M., 2010. Hybrid H-infinity-Based Wavelet-Neural-Network Tracking Control for Permanent-Magnet Synchronous Motor Servo Drives. *IEEE Trans. Ind. Electron.*, 57(9): 3157-3166. https://dx.doi.org/10.1109/Tie.2009.2038331

El-Sousy, F.F.M., 2013. Intelligent Optimal Recurrent Wavelet Elman Neural Network Control System for Permanent-Magnet Synchronous Motor Servo Drive. *IEEE Trans. Ind. Inform.*, 9(4): 1986-2003. https://dx.doi.org/10.1109/Tii.2012.2230638

Feng, G., Liu, Y.F., Huang, L.P., 2004. A new robust algorithm to improve the dynamic performance on the speed control of induction motor drive. *IEEE Trans. Power Electron.*, 19(6): 1614-1627. https://dx.doi.org/10.1109/Tpel.2004.836619

Feng, Y., Han, F.L., Yu, X.H., 2014. Chattering free full-order sliding-mode control. *Automatica*, 50(4): 1310-1314. https://dx.doi.org/10.1016/j.automatica.2014.01.004

Feng, Y., Yu, X.H., Man, Z.H., 2002. Non-singular terminal sliding mode control of rigid manipulators. *Automatica*, 38(12): 2159-2167. https://dx.doi.org/10.1016/S0005-1098(02)00147-4

Han, J.Q., 2009. From PID to Active Disturbance Rejection Control. *IEEE Trans. Ind. Electron.*, 56(3): 900-906. https://dx.doi.org/10.1109/Tie.2008.2011621

Jiang, J.F., Zhou, X.J.,2019. A robust and fast sliding mode controller for position tracking control of permanent magnetic synchronous motor. The 3rd International Conference on Power, Energy and Mechanical Engineering, p. 95–99. https://dx.doi.org/10.1051/e3sconf/20199503002

Li, S.H., Liu, Z.G., 2009. Adaptive Speed Control for Permanent-Magnet Synchronous Motor System With Variations of Load Inertia. *IEEE Trans. Ind. Electron.*, 56(8): 3050-3059. https://dx.doi.org/10.1109/Tie.2009.2024655

Li, S.H., Sun, H.B., Yang, J., et al., 2015. Continuous Finite-Time Output Regulation for Disturbed Systems Under Mismatching Condition. *IEEE Trans. Autom. Contr.*, 60(1): 277-282.

https://dx.doi.org/10.1109/Tac.2014.2324212

Man, Z.H., Paplinski, A.P., Wu, H.R., 1994. A robust MIMO terminal sliding mode control scheme for rigid robotic manipulators. *IEEE Trans. Autom. Contr.*, 39(12): 2464–2469. https://dx.doi.org/10.1109/9.362847

Miklosovic, R., Gao, Z.Q., 2004. A robust two-degree-of-freedom control design technique and its practical application. 39th IAS Annual Meeting on Industry Application Conference, p. 1495–1502. https://dx.doi.org/10.1109/IAS.2004.1348669

Nguyen, A.T., Rafaq, M.S., Choi, H.H., et al., 2018. A Model Reference Adaptive Control Based Speed Controller for a Surface-Mounted Permanent Magnet Synchronous Motor Drive. *IEEE Trans. Ind. Electron.*, 65(12): 9399-9409. https://dx.doi.org/10.1109/Tie.2018.2826480

Nguyen, H.T., Jung, J.W., 2018. Finite Control Set Model Predictive Control to Guarantee Stability and Robustness for Surface-Mounted PM Synchronous Motors. *IEEE Trans. Ind. Electron.*, 65(11): 8510-8519. https://dx.doi.org/10.1109/Tie.2018.2814006

Saadaoui, O., Khlaief, A., Abassi, M., et al., 2017. A sliding-mode observer for high-performance sensorless control of PMSM with initial rotor position detection. *Int. J. Contr.*, 90(2): 393-408. https://dx.doi.org/10.1080/00207179.2016.1181788

Su, J.B., Qiu, W.B., Ma, H.Y., et al., 2004. Calibration-free robotic eye-hand coordination based on an auto disturbance-rejection controller. *IEEE Trans. Robotic Autom.*, 20(5): 899-907. https://dx.doi.org/10.1109/Tro.2004.829458

Su, Y.X., Zheng, C.H., Duan, B.Y., 2005. Automatic disturbances rejection controller for precise motion control of permanent-magnet synchronous motors. *IEEE Trans. Ind. Electron.*, 52(3): 814-823. https://dx.doi.org/10.1109/Tie.2005.847583

Wai, R.J., 2001. Total sliding-mode controller for PM synchronous servo motor drive using recurrent fuzzy neural network. *IEEE Trans. Ind. Electron.*, 48(5): 926-944. https://dx.doi.org/10.1109/41.954557

Wang, H.M., Li, S.H., Lan, Q.X., et al., 2017. Continuous terminal sliding mode control with extended state observer for PMSM speed regulation system. *Trans. Ins. Meas. Contr.*, 39(8): 1195-1204. https://dx.doi.org/10.1177/0142331216630361

Wang, M., Yang, J.Q., Zhang, X., et al., 2018. Accurate two-degree-of-freedom discrete-time current controller design for PMSM using complex vectors. *Front. Inform. Technol. Electron. Eng.*, 19(4): 569-581. https://dx.doi.org/10.1631/fitee.1601390

Wu, D., Chen, K., Wang, X., 2007. Tracking control and active disturbance rejection with application to noncircular machining. *Int. J. Mach. Tool Manu.*, 47(15): 2207-2217. https://dx.doi.org/10.1016/j.ijmachtools.2007.07.002

Yang, J., Li, S.H., Su, J.Y., et al., 2013. Continuous nonsingular terminal sliding mode control for systems with mismatched disturbances. *Automatica*, 49(7): 2287-2291. https://dx.doi.org/10.1016/j.automatica.2013.03.026

Yang, J.Q., Yin, R.S., Zhang, X.J., et al., 2017. Exponential response electrical pole-changing method for a five-phase induction machine with a current sliding mode control strategy. *Front. Inform. Technol. Electron. Eng.*, 18(8): 1151-1166. https://dx.doi.org/10.1631/fitee.1601728

Yu, S.H., Yu, X.H., Shirinzadeh, B., et al., 2005. Continuous finite-time control for robotic manipulators with terminal sliding mode. *Automatica*, 41(11): 1957-1964. https://dx.doi.org/10.1016/j.automatica.2005.07.001

Zeng, Z.L., Cheng, L.M., Qian, L., et al., 2002. A newly robust controller design for the position control of permanent-magnet synchronous motor. *IEEE Trans. Ind. Electron.*, 49(3): 558–565. https://dx.doi.org/10.1109/tie.2002.1005380

Zhang, X.Y., 2016. Application of direct adaptive fuzzy slidingmode control into a class of non-affine discrete nonlinear systems. *Front. Inform. Technol. Electron. Eng.*, 17(12): 1331-1343. https://dx.doi.org/10.1631/fitee.1500318

Zhi, D.W., Xu, L., Williams, B.W., 2010. Model-Based Predictive Direct Power Control of Doubly Fed Induction Generators. *IEEE Trans. Power Electron.*, 25(2): 341-351. https://dx.doi.org/10.1109/Tpel.2009.2028139